Field and current distributions and ac losses in superconducting strips

John R. Clem

Ames Laboratory and Department of Physics and Astronomy, Iowa State University, Ames, Iowa 50011-3160, USA

In this paper I discuss analytic and numerical calculations of the magnetic-field and sheet-current distributions in superconducting strips of width $2a$ and arbitrary thickness $2b$ at the center when the cross-section is an ellipse, a rectangle, and a shape intermediate between these limits. Using critical-state theory, I use several methods to determine the functional dependence of the ac transport-current losses upon $F=I/I_c$, where I is the peak alternating current and I_c is the critical current, and I discuss how this dependence can be affected by the cross-sectional shape, aspect ratio, and a flux-density-dependent critical current density $J_c(B)$.

I. INTRODUCTION

In determining the usefulness of a type-II superconductor in applications, the ac losses are a very important factor. Many composite conductors currently under development for large-scale applications of superconductivity are in the form of tapes, consisting of superconducting strips embedded in a nonsuperconducting metallic matrix. In this paper I focus on the self-field hysteretic ac losses of such superconducting strips carrying an ac, neglecting the possibility of losses in the surrounding matrix.

In a classic paper, Norris[1] investigated the hysteretic ac losses in type-II superconductors with a variety of cross-sections, and he derived results for the ac transport-current losses expressed in powers of $F=I/I_c$, where I is the peak alternating current and I_c is the critical current. For small values of F, Norris found that the losses were proportional to F^3 for wires of elliptical or circular cross-section but were proportional to F^4 for thin strips of rectangular cross-section. The large difference in the power-law behavior seems puzzling in view of the fact that films of elliptical cross-section look very similar to films of rectangular cross-section when both films are thin.

To analyze the reasons for this difference in power-law behavior, there are at least three theoretical questions that need to be addressed. First, how thin must a rectangular strip of width $2a$ and thickness $2b$ be in order for the ac losses to be well described by the thin-film limit studied by Norris? Second, assuming that a film of width $2a$ and thickness $2b$ in the middle is thin enough to be described by the thin-film limit, how do the ac losses depend upon the cross-sectional shape if the cross-section is neither a rectangle nor an ellipse but something in between, as shown in Fig. 1? Third, since the critical current density J_c depends in general upon the local magnetic flux density B, does the B dependence of J_c have a significant effect?

Experimental questions regarding the power-law behavior also have been raised. Some measurements[2,3] of the ac transport-current losses in YBCO films and Bi-2223 tapes have been found to deviate from the F^4 behavior expected for thin strips of rectangular cross-section.

In this paper I theoretically explore how the transport ac losses of a superconducting strip depend upon $F=I/I_c$, and I discuss how this functional dependence can be affected by

the superconductor's cross-sectional shape, aspect ratio, and $J_c(B)$. I begin in Sec. II by discussing ways to calculate the field and current distributions in the critical state. In Sec. II A I discuss thick strips with cross-sections described by a shape function $y_c(x)$, and I model the inner boundary of the flux-penetrated region by a similar function $y_I(x)$. In Sec. II B I present results for the field and current distributions for superconducting strips of different cross-sectional shapes $y_c(x)$ in the thin-film limit. In Sec. III I apply these results to calculate the hysteretic ac transport losses. After discussing some general methods in Sec. III A, I discuss the losses in conductors with elliptical cross-section in Sec. III B and with rectangular cross-section in Sec. III C. For the thin-film limit I calculate the losses in conductors with elliptical, rectangular, and intermediate cross-sections in Sec. III D, and I show how to account approximately for the B dependence of $J_c(B)$ in Sec. III E. Finally, I briefly summarize my results in Sec. IV.

II. FIELD AND CURRENT DISTRIBUTIONS

A. Thick strips

To simplify the calculations and obtain analytic results, Norris used critical-state theory,[4] assuming that the relation between the magnetic induction **B** and the magnetic field **H** is $\boldsymbol{B}=\mu_0\boldsymbol{H}$ and that the critical current density J_c is independent of B. I use the same assumptions here. Norris noted that the ac loss calculation is greatly simplified by first finding the shape of the cross-sectional area of the flux front at the
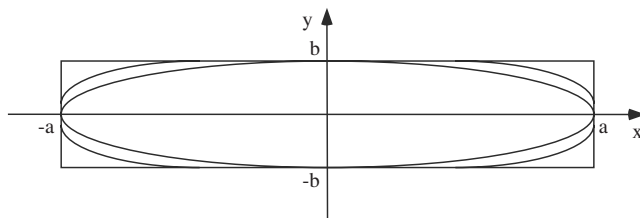

FIG. 1. Cross-sections considered in this paper, all representing superconducting strips of width $2a$ and thickness $d=2b$ at the center: an ellipse of semimajor axis a and semiminor axis b, a rectangle of length $2a$ and height $2b$, and an intermediate shape, described in the text.

peak current I, and he found that for superconductors of elliptical cross-section the flux front is an ellipse with the same aspect ratio as that of the superconductor itself. Although Norris did not report the shape of the flux front for very thin superconductors of rectangular cross-section, the shape can be inferred from the current and field distributions.[5,6] In this paper, I assume a function with two fitting parameters to approximate the flux-front shape. Although this shape function does not yield exact results, the resulting magnetic-field and current distributions are very nearly correct. I then use these distributions to calculate the ac losses.

Sketched in Fig. 1 are the sample cross-sections to be considered in this paper. The boundary surface can be described by $y = \pm y_c(x)$, where

$$y_c(x) = \frac{b \tan^{-1}\sqrt{\alpha^2(1 - x^2/a^2)}}{\tan^{-1} \alpha} \tag{1}$$

or its inverse, $x = \pm x_c(y)$, where

$$x_c(y) = a\sqrt{1 - \frac{1}{\alpha^2}\tan^2\left(\frac{y \tan^{-1} \alpha}{b}\right)} \tag{2}$$

and α is a dimensionless parameter that can range from 0 to ∞. In the limit $\alpha \rightarrow 0$, these equations describe an ellipse of semiaxes a and b; in the limit $\alpha \rightarrow \infty$, they describe a rectangle of dimensions $2a \times 2b$; and for an intermediate value of α, they describe the intermediate shape shown in Fig. 1.

The radius of curvature of the curve $y_c(x)$ at $x = a$ or of $x_c(y)$ at $y = 0$ is

$$R_c = \left(\frac{\alpha}{\tan^{-1} \alpha}\right)^2 \frac{b^2}{a}. \tag{3}$$

For reference, note that $R_c = b$ when $\alpha = 0$ for $b/a = 1$, $\alpha = 4.23$ for $b/a = 0.1$, $\alpha = 15.0$ for $b/a = 0.01$, $\alpha = 49.0$ for $b/a = 0.001$, $\alpha = 156$ for $b/a = 0.0001$, and $\alpha = 496$ for $b/a = 0.00001$.

The cross-sectional area S_c of the sample is

$$S_c = \frac{2\pi ab(\sqrt{1 + \alpha^2} - 1)}{\alpha \tan^{-1} \alpha}, \tag{4}$$

such that $S_c \rightarrow \pi ab$ when $\alpha \rightarrow 0$; $S_c \rightarrow 4ab$ when $\alpha \rightarrow \infty$; and $\pi ab < S_c < 4ab$ when $0 < \alpha < \infty$.

When a uniform current density $J_z = J_c$ is flowing throughout the entire cross-section S_c, the vector potential is $\mathbf{A}_c(x,y) = A_{cz}(x,y)\hat{z}$,

$$A_{cz}(x,y) = -\frac{\mu_0 J_c}{4\pi}\int\int_{S_c} du\,dv\,\log\left[\frac{(x-u)^2 + (y-v)^2}{u^2 + v^2}\right], \tag{5}$$

where the integral over u and v extends over the area S_c and the constant of integration has been chosen such that $A_{cz}(0,0) = 0$. Expressions for $A_{cze}(x,y)$ for the elliptical cross-section and $A_{czr}(x,y)$ for the rectangular cross-section are given in Appendices A and B, but $A_{czi}(x,y)$ for the intermediate case is most conveniently obtained by numerical integration using upper and lower limits obtained from Eq.

(1) or (2). The magnetic induction is $\mathbf{B}_c(x,y) = \mu_0\mathbf{H}_c(x,y) = \nabla \times \mathbf{A}_c(x,y)$.

On the other hand, when a current $I < I_c$ is applied in the z direction to a sample originally in the virgin state containing no magnetic flux, magnetic flux pushes its way into the sample. The leading edge of the flux front encircles an area S_I, here approximated as a roughly elliptical shape of width $2c$ and height $2y_0$, with a boundary in the first quadrant given by equations of the same form as Eqs. (1) and (2)

$$y_I(x) = \frac{y_0 \tan^{-1}\sqrt{\beta^2(1 - x^2/c^2)}}{\tan^{-1} \beta} \tag{6}$$

or its inverse,

$$x_I(y) = c\sqrt{1 - \frac{1}{\beta^2}\tan^2\left(\frac{y \tan^{-1} \beta}{y_0}\right)}, \tag{7}$$

where β is a dimensionless parameter that can range from 0 to ∞. The area enclosed by the flux front is

$$S_I = \frac{2\pi c y_0(\sqrt{1 + \beta^2} - 1)}{\beta \tan^{-1} \beta}. \tag{8}$$

Consider, as an auxiliary function, the vector potential $\mathbf{A}_I(x,y) = A_{Iz}(x,y)\hat{z}$ generated by a uniform current density $J_z = -J_c$ flowing only in the cross-section S_I,

$$A_{Iz}(x,y) = \frac{\mu_0 J_c}{4\pi}\int\int_{S_I} du\,dv\,\log\left[\frac{(x-u)^2 + (y-v)^2}{u^2 + v^2}\right], \tag{9}$$

where the integral over u and v extends over the area S_I, and the constant of integration again has been chosen such that $A_{Iz}(0,0) = 0$. The corresponding magnetic induction is $\mathbf{B}_I(x,y) = \mu_0\mathbf{H}_I(x,y) = \nabla \times \mathbf{A}_I(x,y)$.

When the current $I < I_c$ is applied in the z direction, the current density is $J_z = J_c$ in the area $S_p = S_c - S_I$, the flux-penetrated portion of S_c outside the area S_I, and $J_z = 0$ inside the area S_I. The resulting vector potential $\mathbf{A}(x,y) = A_z(x,y)\hat{z}$ is

$$A_z(x,y) = A_{cz}(x,y) + A_{Iz}(x,y),$$

$$= \frac{\mu_0 J_c}{4\pi}\int\int_{S_p} du\,dv\,\log\left[\frac{(x-u)^2 + (y-v)^2}{u^2 + v^2}\right], \tag{10}$$

subject to the condition that the shape of the area S_I is such that $A_z = 0$ inside the area S_I, and the corresponding magnetic-flux density

$$\mathbf{B}(x,y) = \mathbf{B}_c(x,y) + \mathbf{B}_I(x,y) \tag{11}$$

is also zero there. The reduced current $F = I/I_c$, where $I_c = J_c S_c$, obeys

$$F = S_p/S_c. \tag{12}$$

Norris[1] showed that if the cross-section of the superconductor is an ellipse of semiaxes a and b, such that the bounding surface is described by Eqs. (1) and (2) with $\alpha \rightarrow 0$ and $S_c = \pi ab$, the flux front encloses the area $S_I = \pi c y_0$, an ellipse of semiaxes c and y_0 described by Eqs. (6) and (7) with $\beta \rightarrow 0$, where $y_0/c = b/a$. The reduced current $F = I/I_c$ obeys $F = 1 - c^2/a^2$.
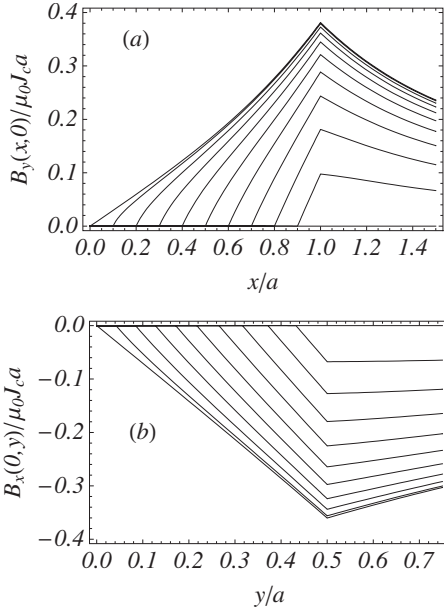
FIG. 2. Plots of (a) $B_y(x,0)/\mu_0 J_c a$ and (b) $B_x(0,y)/\mu_0 J_c a$ vs x/a for $c/a=0$, 0.1, 0.2, 0.3, 0.4, 0.5, 0.6, 0.7, 0.8, 0.9, and 1.0 in a strip of rectangular cross-section of dimensions $2a \times 2b$, where $b=a/2$. The corresponding values of y_0, β, S_I/S_c, and $F=I/I_c$ are given in Table I.

Norris[1] also considered a flat superconducting strip of width $2a$ and thickness $2b \ll 2a$, and obtained the current density averaged over the thickness, which can be written as

$$\bar{J}_z(x) = \frac{2J_c}{\pi}\tan^{-1}\sqrt{\frac{a^2-c^2}{c^2-x^2}}, \quad |x| < c, \tag{13}$$

$$= J_c, \quad c \le |x| \le a, \tag{14}$$

where $F=I/I_c=\sqrt{1-c^2/a^2}$ is the reduced current. Since $\bar{J}_z(x)=J_c[1-y_I(x)/b]$, the area S_I has only a roughly elliptical shape of width $2c$ with upper and lower boundaries at $y=\pm y_I(x)$ as given in Eq. (6), where $\beta^2=c^2/(a^2-c^2)=(1-F^2)/F^2$ and $y_0=(2b/\pi)\tan^{-1}\beta$. When $F \to 0$, $\beta \to \infty$, and S_I becomes a rectangle with width $2a$ and height $2b$, filling the entire cross-section. When $F \to 1$, $\beta \to 0$, and S_I becomes a small ellipse with semimajor axis $c \approx a\sqrt{1-F^2}$ and semiminor axis $y_0 \approx (2b/\pi)\sqrt{1-F^2}$, so that $y_0/c=(\pi/2)b/a$.

To obtain approximate results for the vector potential $A_z(x,y)\hat{z}$ and the corresponding magnetic-flux density $\boldsymbol{B}(x,y)$ for sample cross-sections that are intermediate between an ellipse and a very thin flat strip, we can use the following procedure. When the current $I<I_c$, we assume that the vector potential is given by Eq. (10), where the auxiliary vector potential $A_{Iz}(x,y)$ depends upon the shape S_I, which in turn is characterized by three fitting parameters, c, y_0, and β. For a given value of $F=I/I_c$, we can determine these parameters from three equations, Eq. (12), $B_y(c,0)=0$ and $B_x(0,y_0)=0$.

For a rectangular cross-section we can use Eq. (11), evaluate $\boldsymbol{B}_c(x,y)$ analytically using Appendix B, and calculate $\boldsymbol{B}_I(x,y)$ numerically using Appendix C. Examples of the results of this procedure are shown in Fig. 2, which exhibits

TABLE I. Fitting parameters for S_I (c, y_0, and β), S_I/S_c, and $F=I/I_c$ for the plots shown in Fig. 2 obtained from the requirements that $B_x(0,y_0)=0$ and $B_y(c,0)=0$. The strip has a rectangular cross-section of dimensions $2a \times 2b$, where $b=a/2$, such that $S_c=2a^2$.

c/a	y_0/a	β	S_I/S_c	F
0.0	0.000	0.000	0.000	1.000
0.1	0.042	0.141	0.007	0.993
0.2	0.084	0.290	0.027	0.973
0.3	0.127	0.453	0.061	0.939
0.4	0.171	0.642	0.111	0.889
0.5	0.217	0.878	0.178	0.822
0.6	0.265	1.197	0.267	0.733
0.7	0.316	1.685	0.382	0.618
0.8	0.371	2.596	0.533	0.467
0.9	0.432	5.184	0.731	0.269
1.0	0.500	∞	1.000	0.000

plots of $B_y(x,0)$ and $B_x(0,y)$ vs x for $b/a=1/2$ and a series of values of c/a. When b/a is not very small (as in the case shown), B_y and B_x vary nearly linearly with distance near the sample surface. Table I exhibits the corresponding values of y_0/a, β, S_I/S_c, and $F=I/I_c$. The solid curves in Fig. 3 show plots of $\Delta_x=(a-c)/a$, calculated as above, vs $F=I/I_c$ for a variety of values of b/a. For $F \ll 1$ and modest values of b/a, $\Delta_x \propto F$; note that $\Delta_x \propto F^2$ only for very small values of b/a.

Figure 4 shows a contour plot of $A_z(x,y)$ vs x and y, calculated as described above, for a strip of rectangular cross-section. The contours correspond to magnetic-field lines, which, in principle, do not penetrate into the area S_I bounded by the bold curve. However, the assumed shape of the area S_I as approximated by $y=\pm y_I(x)$ [Eq. (6)] or $x=\pm x_I(y)$ [Eq. (7)] does not give exact solutions for either the vector potential $A_z(x,y)$ or the magnetic induction $\boldsymbol{B}(x,y)=\mu_0\boldsymbol{H}(x,y)$. Nevertheless, for the cases shown in Figs. 2 and 4, the calculated values of $B(x,y)$
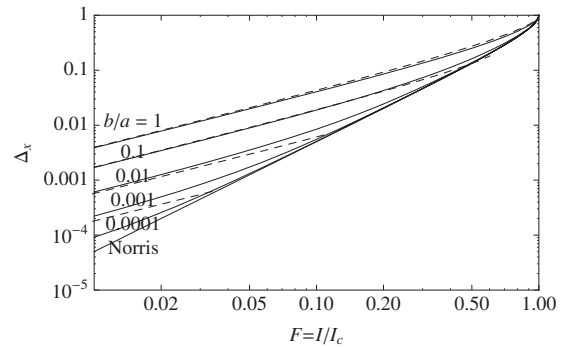

FIG. 3. The upper five solid curves show values of $\Delta_x=(a-c)/a$ vs $F=I/I_c$ for a strip of rectangular cross-section ($2a \times 2b$), numerically calculated as described in the text for $b/a=1$, 0.1, 0.01, 0.001, and 0.0001. The corresponding dashed curves show results using the conformal-mapping method described in Sec. III C 2. The lowest solid curve shows $\Delta_x=1-\sqrt{1-F^2}$, obtained from Eq. (20) in Sec. II B, Norris's result for a very thin strip of rectangular cross-section (Ref. 1).
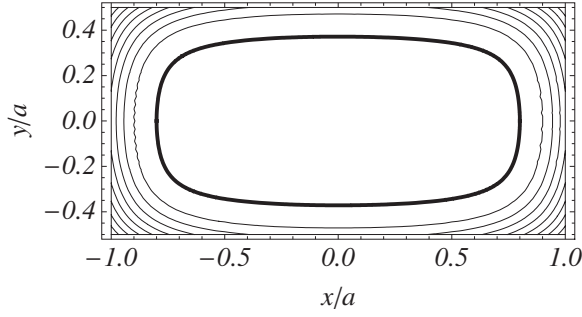
FIG. 4. Contour plot of $A_z(x,y)$ vs x/a and y/a for $c/a=0.8$, $y_0/a=0.372$, $\beta=2.629$, $S_I/S_c=0.534$, and $F=I/I_c=0.466$ in a strip of rectangular cross-section of dimensions $2a \times 2b$, where $b=a/2$. The flux front, described by $y=\pm y_I(x)$ [Eq. (6)] and shown as the bold curve, surrounds the area S_I. The contours correspond to magnetic-field lines, which circulate around S_I in the counterclockwise direction.

$=\sqrt{B_y^2(x,y)+B_x^2(x,y)}$ and $A_z(x,y)$ inside the area S_I, though not precisely equal to zero, are about three or four orders of magnitude smaller than their values on the perimeter of the strip. These results indicate that the values of $A_z(x,y)$ or the magnetic induction $\boldsymbol{B}(x,y)=\mu_0 \boldsymbol{H}(x,y)$ calculated as above are reasonable approximations to the exact solutions, thereby permitting relatively simple calculations showing how hysteretic ac losses depend upon the cross-sectional shape.

B. Thin-film limit

The magnetic fields generated by long thin strips can be calculated as in Refs. 1, 5, and 6, using the method of complex fields. Instead of dealing with the vector field $\boldsymbol{H}(x,y)$ $=\boldsymbol{B}(x,y)/\mu_0=\hat{x}H_x(x,y)+\hat{y}H_y(x,y)$, one works with the complex field $\mathcal{H}(\zeta)=H_y+iH_x$, which is an analytic function of $\zeta=x+iy$ outside the strip. Since analytic functions obey the Cauchy relations, the conditions that $\nabla \cdot \boldsymbol{H}=0$ and $\nabla \times \boldsymbol{H}=0$ are automatically satisfied.

In the limit as $b/a \to 0$, the complex magnetic field outside a thin strip whose boundary surface is described by Eq. (1) and which carries a total current I with a current density $J_z=J_c$ at the edges $(c \le |x| < a)$ and an average current density $\bar{J}_z(x)<J_c$ in the middle $(|x|<c)$ is

$$\mathcal{H}(\zeta)=\frac{J_c b}{\tan^{-1}\alpha}\left[\tanh^{-1}\left(\frac{\alpha\sqrt{\tilde{\zeta}^2-\tilde{c}^2}}{\sqrt{1+\alpha^2(1-\tilde{c}^2)}}\right)\right.$$
$$\left.-\tanh^{-1}(\alpha\sqrt{\tilde{\zeta}^2-1})\right], \qquad (15)$$

where $\tilde{\zeta}=\zeta/a$ and $\tilde{c}=c/a$. The condition relating I and c is

$$F=\frac{I}{I_c}=\frac{\sqrt{1+\alpha^2(1-\tilde{c}^2)}-1}{\sqrt{1+\alpha^2}-1}, \qquad (16)$$

where $I_c=J_c S_c$ [see Eq. (4)]. Here $\sqrt{\tilde{\zeta}^2-\tilde{c}^2}$ means $(\tilde{\zeta}-\tilde{c})^{1/2}(\tilde{\zeta}+\tilde{c})^{1/2}$.
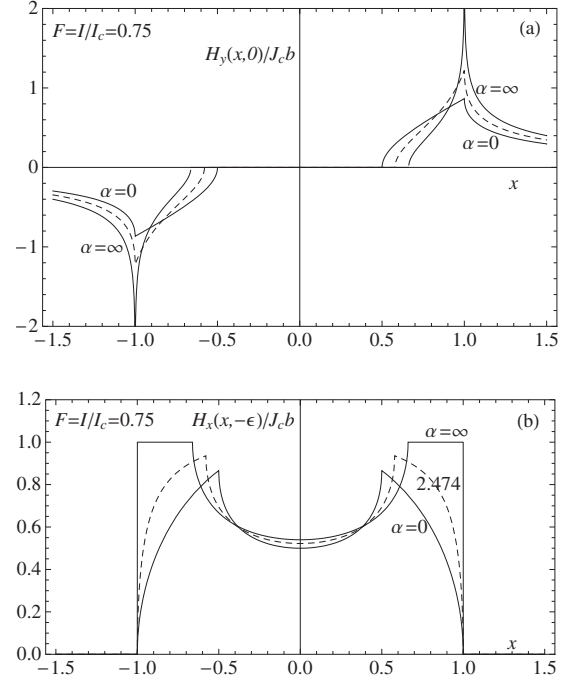
Equations (15) and (16) reduce to

FIG. 5. Plots of $H_y(x,0)$ and $H_x(x,-\epsilon)$ (on the bottom of the strip) calculated from Eqs. (15)–(20) for $a=1$, $\alpha=0$, 2.474 (dashed), and ∞, and $F=I/I_c=0.75$, for which $c/a=0.500$, 0.579, and 0.661.

$$\mathcal{H}(\zeta)=J_c b(\sqrt{\tilde{\zeta}^2-\tilde{c}^2}-\sqrt{\tilde{\zeta}^2-1}), \qquad (17)$$

$$F=1-\tilde{c}^2 \qquad (18)$$

for an elliptical cross-section $(\alpha=0)$ and to

$$\mathcal{H}(\zeta)=\frac{2J_c b}{\pi}\tanh^{-1}\sqrt{\frac{1-\tilde{c}^2}{\tilde{\zeta}^2-\tilde{c}^2}}, \qquad (19)$$

$$F=\sqrt{1-\tilde{c}^2} \qquad (20)$$

for a rectangular cross-section $(\alpha=\infty)$.

Shown in Fig. 5 are plots of $H_y(x,0)$ and $H_x(x,-\epsilon)$ obtained from Eqs. (15)–(20) for $F=I/I_c=0.75$ and $\alpha=0$ (solid curves), 2.474 (dashed), and ∞ (solid). The cross-sectional area for $\alpha=2.474$ is $3.57ab$, the average of the areas of an ellipse (πab) and a rectangle $(4ab)$. In the regions $c \le |x| < a$, $J_z=J_c$, and $H_x(x,-\epsilon)=J_c y_c(x)$ [see Eq. (1)].

III. AC LOSSES

A. Methods

We are now in a position to analyze some general features of the hysteretic transport ac losses in isolated superconducting strips. Let us consider ac of amplitude I less than I_c at frequencies $f=1/T$ that are sufficiently low that eddy-current losses are negligible and the losses can be calculated using a quasistatic approach.[1] The solutions for $\boldsymbol{B}(x,y)=\mu_0 \boldsymbol{H}(x,y)$ derived in Sec. II can be used to calculate Q', the energy dissipated per cycle per unit length. Consider time $t=0$, when the current has its maximum value I in the z direction,

the magnetic-field distribution is given by $\mathbf{H}(x,y) = \hat{x}H_x(x,y) + \hat{y}H_y(x,y)$, the magnetic induction is $\mathbf{B}(x,y) = \mu_0\mathbf{H}(x,y)$, and the vector potential is $\mathbf{A}(x,y) = A_z(x,y)\hat{z}$. Half a cycle earlier, at time $t = -T/2$, when the current was in the opposite direction, $\mathbf{B}(x,y,-T/2) = -\mu_0\mathbf{H}(x,y)$. The loss per cycle per unit length Q' is twice the loss in the half cycle $-T/2 \le t \le 0$. Thus

$$Q' = 2\int_{-T/2}^{0} dt \int\int_{S_c} dxdy J_z(x,y,t)E_z(x,y,t). \qquad (21)$$

According to critical-state theory,[4] during this time interval, E_z is nonzero only where J_z is just above J_c, such that J_z can be replaced by J_c in Eq. (21), but the integral is to be carried out only over those portions of the flux-penetrated cross-section S_p, where $\mathbf{B} = \nabla \times \mathbf{A}$ is changing with time and $E_z(x,y,t) > 0$. Note that, if S_I is chosen correctly, $E_z = 0$ throughout the entire area S_I and we may therefore chose a gauge such that $A_z = 0$ there. Next, we can use Faraday's law in the form $\oint d\mathbf{l}\cdot\mathbf{E} = -\int d\mathbf{S}\cdot\partial\mathbf{B}/\partial t = -\int d\mathbf{S}\cdot\partial(\nabla\times\mathbf{A})/\partial t$, where the surface S is a rectangle with the sides L_z parallel to the z axis and the ends extending from the origin to (x,y) in the flux-penetrated region. Application of Stokes's theorem thus yields

$$E_z(x,y,t) = -\partial A_z(x,y,t)/\partial t. \qquad (22)$$

Substituting this expression into Eq. (21), integrating over time, noting that the change in the vector potential is $A_z(x,y,0) - A_z(x,y,-T/2) = 2A_z(x,y)$, we obtain

$$Q' = -4J_c\int\int_{S_p} dxdy A_z(x,y). \qquad (23)$$

(Since the current I is in the positive z direction at time $t = 0$, $A_z(x,y) < 0$ outside the area S_I.) The areal density of energy dissipated per unit length during one cycle therefore can be expressed as $q'(x,y) = 4J_c|A_z(x,y)|$. For example, for a strip of rectangular cross-section, we can see from the contour plot of $A_z(x,y)$ in Fig. 4 that the largest values of $q'(x,y)$ occur at the four corners.

To compare the losses in strips with the same critical current I_c but different cross-sections, it is useful to express Q' in terms of a dimensionless geometry-dependent loss function $L(F)$, which is a function of $F = I/I_c$,

$$Q' = \mu_0 I_c^2 L(F), \qquad (24)$$

$$L(F) = \frac{1}{S_c}\int\int_{S_p} dxdy \Lambda(x,y), \qquad (25)$$

$$\Lambda(x,y) = -4A_z(x,y)/\mu_0 I_c. \qquad (26)$$

Note that $\Lambda(x,y)$ is proportional to the local density of time-averaged energy dissipation.

The maximum hysteretic transport losses occur for $I = I_c$ or $F = 1$, when the flux front first touches the axis and S_I shrinks to zero. For a strip with elliptical cross-section, as shown by Norris,[1]
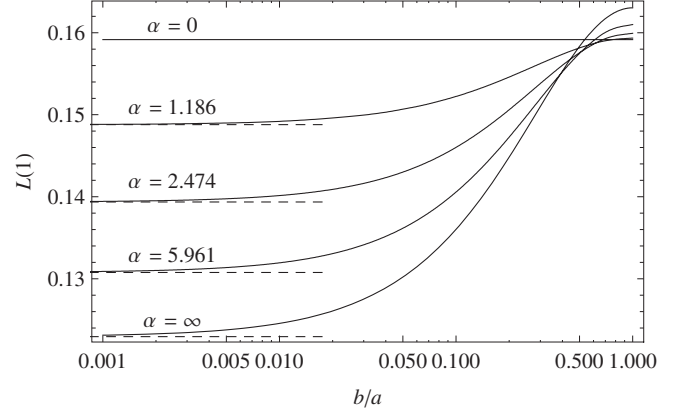

FIG. 6. Plots of $L(1)$ vs b/a at $I = I_c$ calculated from Eqs. (4), (5), and (25)–(28) for $\alpha = 0$ (elliptical cross-section, $S_c = 3.14ab$), values of α corresponding to intermediate shapes and cross-sectional areas (see Fig. 1), $\alpha = 1.186$ ($S_c = 3.36ab$), $\alpha = 2.474$ ($S_c = 3.57ab$), $\alpha = 5.961$ ($S_c = 3.79ab$), and $\alpha = \infty$ (rectangular cross-section, $S_c = 4ab$). The cross-sectional area for $\alpha = 2.474$ is the average of the areas of the elliptical and rectangular cross-sections. For small b/a the curves asymptotically approach the corresponding thin-film limits calculated in Sec. III D, shown as dashed lines.

$$L_e(1) = 1/2\pi = 0.159, \qquad (27)$$

independent of the ratio b/a. For a strip with rectangular cross-section, as shown by Rhyner,[7]

$$L_r(1) = [6\ln 4 - 7 - \tilde{b}^2 \ln(1 + \tilde{b}^{-2}) - \tilde{b}^{-2} \ln(1 + \tilde{b}^2)$$
$$+ 2(\tilde{b}\tan^{-1}\tilde{b}^{-1} + \tilde{b}^{-1}\tan^{-1}\tilde{b})]/6\pi, \qquad (28)$$

where $\tilde{b} = b/a$. For a square cross-section ($b = a$), $L(1) = 0.163$, and for $b/a \ll 1$, $L(1) = 0.123$, in agreement with Rhyner's results of Ref. 7 but in disagreement with Norris's results in Table II of Ref. 1. Shown in Fig. 6 are calculated values of $L(1)$ vs b/a for various cross-sectional shapes characterized by the value of α in Eq. (4). When $b = a$, $L(1) > 0.159$ for all $\alpha > 0$, with the greatest deviation occurring for a square cross-section ($\alpha = \infty$). On the other hand, when $b \ll a$, $L(1) < 0.159$ for all $\alpha > 0$, with the greatest deviation again occurring for a square cross-section.

Another way to express the ac loss per cycle is to start from Eq. (23), use the symmetries $A_z(-x,y) = A_z(x,-y) = A_z(x,y)$, note that $A_z(x,y) = 0$, $B_x(x,y) = 0$, and $B_y(x,y) = 0$ inside S_I, integrate over y in the first quadrant, and carry out partial integrations using $B_x = \partial A_z/\partial y$ and $B_y = -\partial A_z/\partial x$. Equation (24) then can be evaluated using

$$L(F) = L_x(F) + L_y(F), \qquad (29)$$

$$L_x(F) = p\int_0^a dx \int_{y_l(x)}^{y_c(x)} dy [y_c(x) - y][-B_x(x,y)], \qquad (30)$$

$$L_y(F) = p\int_c^a dx G(x)B_y(x,0), \qquad (31)$$

where

$$p = \frac{16}{\mu_0 J_c S_c^2}, \tag{32}$$

$$y_l(x) = y_I(x), \quad 0 \le x < c, \tag{33}$$

$$= 0, \quad c \le x \le a, \tag{34}$$

$$G(x) = \int_x^a dx' y_c(x'). \tag{35}$$

Note that L_y describes the dissipation due to magnetic flux in the form of vortex or antivortex segments perpendicular to the strip transporting flux density B_y in from the edges at $x = \pm a$, while L_x describes the dissipation due to magnetic flux in the form of vortex or antivortex segments parallel to the strip transporting flux density B_x in from the top and bottom surfaces.

The ratio $f_y(F) = L_y(F)/L(F)$ is an increasing function of $F = I/I_c$ and a decreasing function of $\tilde{b} = b/a$. Since for a fixed value of F, $f_y(F) \to 1$ as $b/a \to 0$, Eq. (31) can be used to evaluate $L(F)$ in the thin-film limit, as shown later in Fig. 9.

B. Elliptical cross-section

1. B_y contribution

As shown in Ref. 1, the total hysteretic ac losses of a conductor of elliptical cross-section have the same remarkably simple form for all values of the ratio b/a,[1]

$$L(F) = [(1-F)\ln(1-F) + (2-F)F/2]/\pi, \tag{36}$$

where $F = I/I_c$. The fraction $f_y(F) = L_y(F)/L(F)$ easily can be evaluated numerically for a strip of elliptical cross-section using Eq. (31) and expressions for $B_y(x,0)$ given in Ref. 1, which yield

$$L_y(F) = \frac{8}{\pi^2(1-\tilde{b}^2)} \int_{\tilde{c}}^1 d\tilde{x}(\cos^{-1}\tilde{x} - \tilde{x}\sqrt{1-\tilde{x}^2})$$
$$\times (\sqrt{\tilde{x}^2 - \tilde{c}^2(1-\tilde{b}^2)} - \tilde{b}\tilde{x}). \tag{37}$$

For a strip with elliptical cross-sections $\tilde{c}$ and F are related via $\tilde{c} = c/a = \sqrt{1-F}$.[1] The behavior of $f_y(F)$ vs F is shown in Fig. 7 for various values of $\tilde{b} = b/a$

2. Behavior for small F

Expansion of Eq. (36) in powers of F yields

$$L(F) = \frac{F^3}{6\pi}\left(1 + \frac{1}{2}F + \frac{3}{10}F^2 + \cdots\right). \tag{38}$$

The leading term in this expansion can be obtained most simply as follows. In the Meissner state, the tangential magnetic field at the surface of an infinitely long cylinder of semimajor and semiminor axes a and b carrying current I in the z direction is[8]
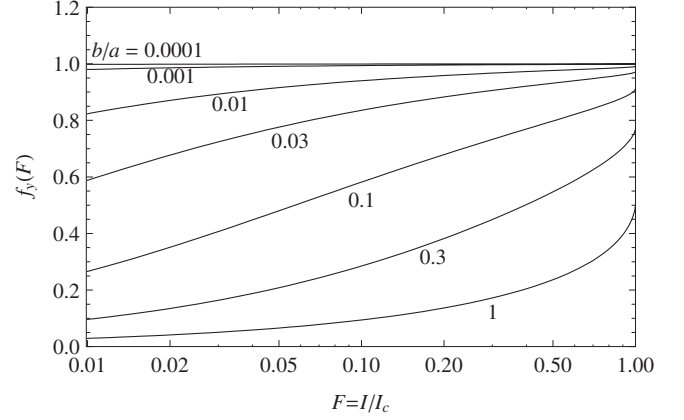

FIG. 7. Plots of the loss fraction $f_y(F) = L_y(F)/L(F)$ vs $F = I/I_c$ calculated from Eqs. (36) and (37) for $b/a = 0.0001$, 0.001, 0.01, 0.03, 0.1, 0.3, and 1 for conductors with an elliptical cross-section ($\alpha = 0$).

$$H_{ts}(\theta') = \frac{I}{2\pi\sqrt{(a\sin\theta')^2 + (b\cos\theta')^2}}, \tag{39}$$

where a point on the surface of the ellipse is described by $(x,y) = (a\cos\theta', b\sin\theta')$. If the self-field at the surface is much larger than H_{c1} (or if we assume that H_{c1} is negligibly small), then according to critical-state theory, magnetic flux will penetrate to a distance $L_p(\theta') = H_{ts}(\theta')/J_c$ from the surface, assuming that $L_p(\theta')$ is much smaller than the corresponding radius of curvature of the surface,

$$\rho(\theta') = [(a\sin\theta')^2 + (b\cos\theta')^2]^{3/2}/ab. \tag{40}$$

When a type-II superconductor is subjected to a parallel ac field of amplitude H_0, the hysteretic ac loss per unit area per cycle is known to be[4]

$$Q_A = \frac{2\mu_0 H_0^3}{3J_c}. \tag{41}$$

Thus the hysteretic ac loss per cycle per unit length of elliptical cylinder can be calculated to lowest order in F using

$$Q' = \oint dl \frac{2\mu_0 H_{ts}^3(\theta')}{3J_c}. \tag{42}$$

where $dl = \sqrt{(a\sin\theta')^2 + (b\cos\theta')^2}\,d\theta'$ is the element of arc length. The integral can be carried out without difficulty, yielding

$$Q' = \mu_0 I_c^2 \left(\frac{F^3}{6\pi}\right), \tag{43}$$

where $I_c = \pi ab J_c$, which agrees with the Norris result to lowest order in F. Application of the condition that $L_p(\theta') \ll \rho(\theta')$ at $\theta' = 0$ is equivalent to the requirement that $F \ll (b/a)^2$ for the derivation of Eq. (43) to be valid. Nevertheless, the Norris derivation, yielding the same F^3 behavior for small F, is not subject to this stringent limitation but instead yields the same result for all values of b/a whenever $F \ll 1$.

C. Rectangular cross-section

1. F^3 or F^4?

Consider a strip of width $2a$ and arbitrary thickness $2b$ in the middle, as shown in Fig. 1. According to critical-state theory, for small values of $F=I/I_c$, magnetic flux penetrates only to a small depth $L_p=H_{ts}/J_c$, where H_{ts} is the self-field tangent to the surface. The flux-penetrated cross-sectional area S_p then can be thought of as a band with a geometry-dependent width that is proportional to F and with a total length equal to the perimeter of the strip. Note also that within S_p, B varies linearly and A_z varies quadratically as a function of the distance from S_I such that the integral of A_z over the cross-section should vary as F^3. Alternatively, the hysteretic ac loss per cycle per unit length can be calculated to good accuracy by using Eq. (41), replacing H_0 by H_{ts}, and integrating around the circumference of the strip. The hysteretic ac loss per cycle per unit length Q' (and hence the loss function L) should always vary as F^3 for small F. How, therefore, can we explain the Norris result for thin strips of rectangular cross-section,[1]

$$L(F) = [(1-F)\ln(1-F) + (1+F)\ln(1+F) - F^2]/\pi, \tag{44}$$

which has the limiting behavior

$$L(F) = F^4/6\pi \tag{45}$$

for small F?

In short, the explanation is that although the losses are indeed approximately proportional to F^3 for small F, the values of F for which the F^3 behavior holds in a thin film of rectangular cross-section are very small. Of the terms in Eqs. (29)–(31), the F^3 behavior for small F arises from $L_x \sim (b/a)F^3$, while $L_y \sim F^4$. Roughly speaking, L_x becomes negligible relative to L_y when $F \gg b/a$. Thus, if one considers values of $F > 0.01$ for samples of rectangular cross-section with $b/a \leq 0.0001$, the losses due to the penetration of B_x into the top and bottom surfaces, as described by L_x, are much smaller than the losses due to penetration of B_y in from the edges, as described by L_y.

2. Conformal-mapping method

To describe the losses for small F, a calculation similar to that described in Eqs. (39)–(43) in Sec. II can be carried out for an infinitely long cylinder of rectangular cross-section with width $2a$ and height $2b$. In this case the tangential magnetic field at the surface, derived using conformal-mapping methods[8–10] and the Schwarz-Christoffel transformation,[10,11] is

$$H_{ts}(\theta') = \frac{I}{2\pi\gamma|\sin^2 \theta' - \sin^2 \beta'|^{1/2}}, \tag{46}$$

where $\cos \beta'=k$, $\sin \beta'=k'=\sqrt{1-k^2}$,

$$a/\gamma = f = E(k) - k'^2 K(k), \tag{47}$$

$$b/\gamma = f' = E(k') - k^2 K(k'), \tag{48}$$

where $K(k)$ is the complete elliptic integral of the first kind of modulus k and complementary modulus $k'=\sqrt{1-k^2}$, $E(k)$ is the complete elliptic integral of the second kind, and an element of arc length around the perimeter is $dl=\gamma|\sin^2 \theta' - \sin^2 \beta'|^{1/2}d\theta'$, starting with $(x,y)=(a,0)$, where $\theta'=0$. At $(x,y)=(a,b)$, $\theta'=\beta'$, and at $(x,y)=(0,b)$, $\theta'=\pi/2$. Assuming that magnetic flux penetrates to a depth $L_p(\theta')=H_{ts}(\theta')/J_c$, using Eqs. (41) and (42), and noting that all four quadrants give equal contributions, we obtain the following integral yielding the hysteretic ac loss per cycle per unit length:

$$Q' = \frac{\mu_0 I^3}{3\pi^3 J_c \gamma^2} \int_0^{\pi/2} \frac{d\theta'}{|\sin^2 \theta' - \sin^2 \beta'|}. \tag{49}$$

However, at $\theta'=\beta'$, the corner $(x,y)=(a,b)$ of the rectangle, the integrand has an unphysical divergence, which needs to be cutoff. Physically, the flux fronts penetrating from the side $x=a$ and the top $y=b$ intersect at points near the corner corresponding to $\theta'=\beta' \pm \delta$, where

$$\delta = \left[\frac{9}{8kk'} \left(\frac{L_{pm}}{\gamma} \right)^2 \right]^{1/3} \ll 1 \tag{50}$$

and $L_{pm}=L_p(\beta' \pm \delta)$. Using Eq. (39) and eliminating L_{pm} in favor of $F=I/I_c$, where $I_c=4abJ_c=4\gamma^2 ff' J_c$, we obtain

$$\delta = \left(\frac{3ff'}{2\pi kk'} F \right)^{1/2} \ll 1. \tag{51}$$

Integrating Eq. (49) over θ' from 0 to $\beta'-\delta$ to obtain the losses on the right side, replacing the integrand by its value at $\beta' \pm \delta$ over the range $\beta'-\delta < \theta' < \beta'+\delta$ to approximate the losses in the corner, integrating Eq. (49) over θ' from $\beta'-\delta$ to $\pi/2$ to obtain the losses on the top, and assuming $\delta \ll 2kk'$ yields

$$Q' = \mu_0 I_c^2 L_{rect}^{(1)}(F), \tag{52}$$

where

$$L_{rect}^{(1)}(F) = \frac{2ff'F^3}{3\pi^3 kk'} \left[2 + \ln \left(\frac{8\pi k^3 k'^3}{3ff'F} \right) \right]. \tag{53}$$

The constant term within the brackets is the corner contribution and the logarithmic term arises from two equal contributions from the length b on the side and the length a on the top. Equation (53) should be a good approximation for small values of F obeying Eq. (51).

The dashed curves in Fig. 3 show values of $\Delta_x = (a-c)/a$ vs F calculated using the above procedure, where $(a-c)$ is the depth of penetration of the flux front measured along the x axis from the surface at $x=a$. The agreement with the solid curves is best for the larger values of b/a. However, the cutoff procedure to account approximately for the otherwise divergent magnetic fields at the corners leads to poorer agreement for small values of b/a, when the corner regions occupy a larger fraction of the cross-section.

The upper solid curves in Fig. 8 show plots of $L_{rect}^{(1)}(F)$ vs F for small F before the curves intersect with the Norris thin-film result for $L(F)$, Eq. (44). For comparison, the
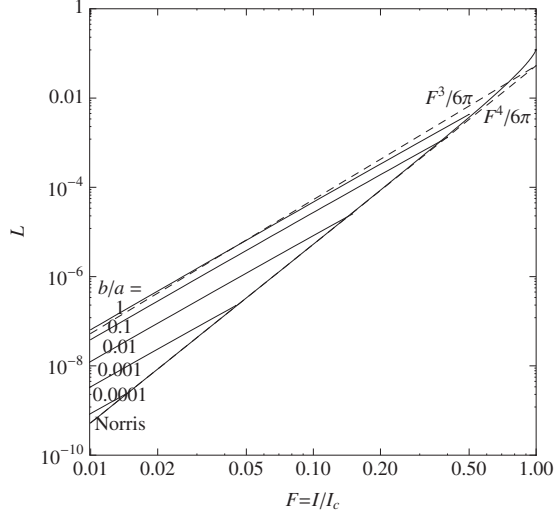
FIG. 8. The upper solid curves display plots of the loss function L vs $F=I/I_c$ calculated from Eq. (53) for a strip of rectangular cross-section with relative dimensions $b/a=1$, 0.1, 0.01, 0.001, and 0.0001. The bottom solid curve shows the Norris result [Eq. (44)] for a very thin strip of rectangular cross-section. For comparison, the upper dashed line shows $F^3/6\pi$ and the lower dashed curve shows $F^4/6\pi$.

dashed curves show the small-F limits $F^3/6\pi$ for the elliptical cross-section, Eq. (38), and $F^4/6\pi$ for thin strips of rectangular cross-section, Eq. (45). Since the logarithmic factor in Eq. (53) is slowly varying, the behavior of the hysteretic losses in a long strip of rectangular cross-section must always behave approximately as $L \propto F^3$ for sufficiently small F, as is evident from Fig. 8.

We can extend the above approach to somewhat larger values of F as follows. We first focus on the flux front that penetrates from the top $y=b$. In terms of the auxiliary variable θ_t', when $\beta' \le \theta_t' \le \pi/2$, the x and y coordinates of a point on the top flux front in units of a are

$$\tilde{x}_t(\theta_t') = [E(\phi,k) - k'^2 F(\phi,k)]/f, \qquad (54)$$

$$\tilde{y}_t(\theta_t') = \frac{f'}{f} - \frac{2f'F}{\pi(\sin^2 \theta_t' - \sin^2 \beta')^{1/2}}, \qquad (55)$$

where $\tilde{x}_t(\theta_t')=x_t(\theta_t')/a$, $\tilde{y}_t(\theta_t')=y_t(\theta_t')/a$, $F=I/I_c$, $F(\phi,k)$ is the normal elliptic integral of the first kind[12,13] of amplitude $\phi=\arcsin(\cos \theta_t'/\cos \beta')$, modulus k, and complementary modulus $k'=\sqrt{1-k^2}$, and $E(\phi,k)$ is the normal elliptic integral of the second kind. We next characterize the flux front that penetrates from the side $x=a$. In terms of the auxiliary variable θ_s', when $0 \le \theta_s' \le \beta'$, the x and y coordinates of a point on the side flux front in units of a are

$$\tilde{x}_s(\theta_s') = 1 - \frac{2f'F}{\pi(\sin^2 \beta' - \sin^2 \theta_s')^{1/2}}, \qquad (56)$$

$$\tilde{y}_s(\theta_s') = [E(\phi',k') - k^2 F(\phi',k')]/f, \qquad (57)$$

where $\tilde{x}_s(\theta_s')=x_s(\theta_s')/a$, $\tilde{y}_s(\theta_s')=y_s(\theta_s')/a$, and where $\phi'=\arcsin(\sin \theta_s'/\sin \beta')$. The top flux front and the side flux

front intersect when $\theta_t' = \theta_{tx}'$ and $\theta_s' = \theta_{sx}'$, where θ_{tx}' and θ_{sx}' are the solutions of the following two equations:

$$\tilde{x}_t(\theta_t') = \tilde{x}_s(\theta_s') = \tilde{x}_{cross}, \qquad (58)$$

$$\tilde{y}_t(\theta_t') = \tilde{y}_s(\theta_s') = \tilde{y}_{cross}, \qquad (59)$$

where $\tilde{x}_{cross}$ and $\tilde{y}_{cross}$ are the x and y coordinates of the crossing point in units of a. Equations (58) and (59) always have physically reasonable solutions for sufficiently small values of $F=I/I_c$.

The corresponding approximation to the ac loss per cycle per unit length can be obtained by integrating Eq. (49) over θ' from 0 to θ_{sx}' to obtain the losses on the right side, replacing the integrand over the range $\theta_{sx}' < \theta' < \theta_{tx}'$ by the average of the values at θ_{sx}' and θ_{tx}' to approximate the losses in the corner, and integrating Eq. (49) over θ' from θ_{tx}' to $\pi/2$ to obtain the losses on the top. The result is

$$Q' = \mu_0 I_c^2 L_{rect}^{(2)}(F), \qquad (60)$$

where

$$
\begin{aligned}
L_{rect}^{(2)}(F) = \frac{4ff'F^3}{3\pi^3} & \left[\frac{1}{kk'} \tanh^{-1}\left(\frac{\tan \theta_{sx}'}{\tan \beta'} \right) \right. \\
& + \frac{(\theta_{tx}' - \theta_{sx}')}{2}\left(\frac{1}{\sin^2 \beta' - \sin^2 \theta_{sx}'} \right. \\
& \left. + \frac{1}{\sin^2 \theta_{tx}' - \sin^2 \beta'} \right) + \frac{1}{kk'}\coth^{-1}\left(\frac{\tan \theta_{tx}'}{\tan \beta'} \right) \left. \right].
\end{aligned}
$$

$$(61)$$

Values of the losses calculated from Eq. (61) are slightly larger that those from Eq. (53), but on Fig. 8 the two curves are indistinguishable.

3. Numerical calculations

Shown in Fig. 9 are plots of $L(F)$ vs F numerically calculated from Eqs. (29)–(35), where the parameters c, y_0, and β were obtained by simultaneously solving Eq. (12), $B_y(c,0)=0$ and $B_x(0,y_0)=0$. The curves of $L(F)$ vs F behave approximately as $L \propto F^3$ for all values of b/a for sufficiently small F. However, as b/a decreases, the curves of $L(F)$ merge into the curve Norris[1] obtained for a very thin strip of rectangular cross-section, Eq. (44), which varies approximately as F^4. The smaller the value of b/a, the smaller the value of F at which the curves merge. For example, the numerically calculated value of $L(F)$ falls within 2% of the Norris result, Eq. (44), when $F>0.93$ for $b/a=0.01$, when $F>0.41$ for $b/a=0.001$, when $F>0.15$ for $b/a=0.0001$, and when $F>0.05$ for $b/a=0.00001$.

However, a comparison of the plots in Figs. 8 and 9 reveals that for small values of F, where the conformal-mapping result for $L(F)$ in Eq. (53) is expected to be most accurate, the numerically calculated values of $L(F)$ shown in Fig. 9 are roughly a factor of two larger than the conformal-mapping result for $L(F)$ shown in Fig. 8. The reason for this is that the assumed form for the flux front in Eq. (6) yields a depth of magnetic-flux penetration L_p near the corners at
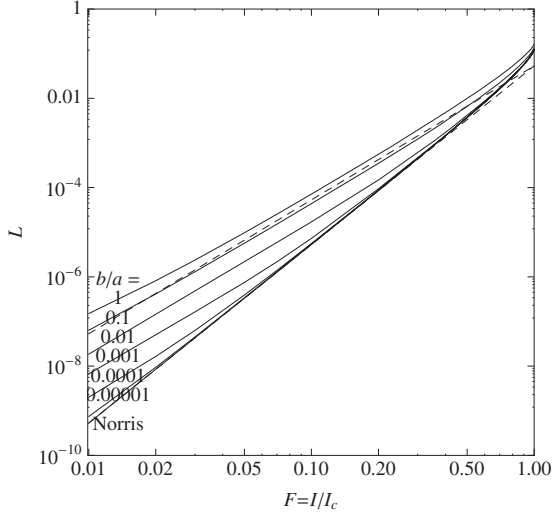
FIG. 9. The upper solid curves display plots of the loss function L vs $F=I/I_c$ numerically calculated from Eqs. (29)–(35) for a strip of rectangular cross-section with relative dimensions $b/a=1$, 0.1, 0.01, 0.001, 0.0001, and 0.00001. The bottom solid curve shows the Norris result [Eq. (44)] for a very thin strip of rectangular cross-section. For comparison, the upper dashed line shows $F^3/6\pi$ and the lower dashed curve shows $F^4/6\pi$.

$(x,y) \approx (\pm a, \pm b)$ that is unrealistically large for small values of F. Since the tangential field at the surface $H_{ts} \approx J_c L_p$ is correspondingly too large, and since the dissipation per cycle per unit area of surface is approximately proportional to H_{ts}^3 [see Eq. (41)], the dissipation per cycle per unit length, obtained by integrating around the circumference of the sample, is also too large.

The main story told by the results displayed in Figs. 8 and 9 is that in a strip of rectangular cross-section the loss function $L(F)$ is approximately proportional to F^3 for small F when b/a is on the order of unity, but as b/a decreases, the F^3 behavior moves to smaller values of F, opening up a
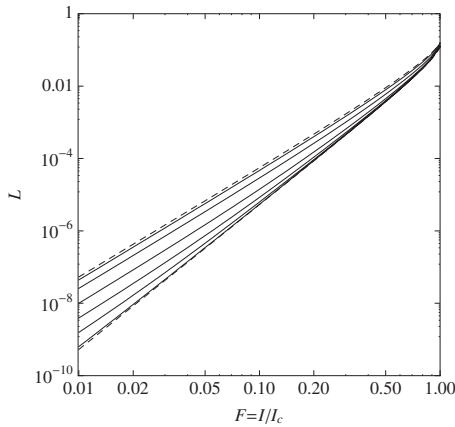

FIG. 10. Plots of the loss function L vs $F=I/I_c$ in the thin-film limit calculated from Eq. (62) for strips of different cross-sectional shapes characterized by the parameter $\alpha=1$, 3, 10, 30, 100, and 1000 (top to bottom) in Eq. (1). The top dashed curve shows the Norris result for an elliptical cross-section [Eq. (36)], and the bottom dashed curve shows the Norris result for a thin strip of rectangular cross-section [Eq. (44)] (Ref. 1).
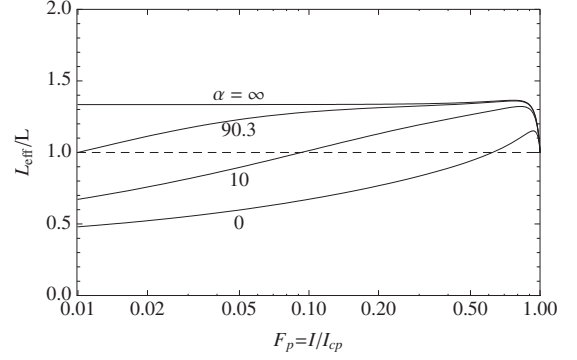

FIG. 11. The solid curves show plots of $L_{eff}(F_p)/L(F_p)$ for $\gamma=10$ and values of $\alpha=0$ (elliptical cross-section), 10, 90.3, and ∞ (rectangular cross-section) in the thin-film limit, where $L_{eff}(F_p)$ is given by Eq. (71) and $L(F_p)$ by Eq. (62). The dashed line shows the corresponding ratios when $\gamma=0$ and J_c is independent of B.

range of F values for which $L(F)$ is approximately proportional to F^4.

D. Thin-film limit

We now calculate the hysteretic loss per cycle per unit length Q' and the loss function L making use of the thin-film-limit approximation that the contribution due to L_x is negligible relative to that due to L_y. Using Eqs. (15) and (31)–(35), we find that the loss function for a thin film described by Eq. (1) with the shape parameter α can be obtained from

$$L(F) = C \int_{\tilde{c}}^{1} d\tilde{x} \mathcal{F}(\tilde{x}) \widetilde{B}_y(\tilde{x},0), \tag{62}$$

where

$$C = \left[\frac{2\alpha}{\pi(\sqrt{1+\alpha^2}-1)} \right]^2, \tag{63}$$

$$\mathcal{F}(\tilde{x}) = \frac{\sqrt{1+\alpha^2}}{\alpha} \cos^{-1}\left(\frac{\tilde{x}}{\sqrt{1+\alpha^2(1-\tilde{x}^2)}} \right) - \frac{1}{\alpha}\cos^{-1}\tilde{x}$$
$$- \tilde{x}\tan^{-1}(\alpha\sqrt{1-\tilde{x}^2}), \tag{64}$$

$$\widetilde{B}_y(\tilde{x},0) = \tanh^{-1}\left[\frac{\alpha\sqrt{\tilde{x}^2-\tilde{c}^2}}{\sqrt{1+\alpha^2(1-\tilde{c}^2)}} \right], \tag{65}$$

$\tilde{x}=x/a$, $\tilde{c}=c/a$, and $\tilde{c}$ is related to $F=I/I_c$ via Eq. (16). For $\alpha=0$ and ∞, the integral can be evaluated analytically and the results for $L(F)$ are the same as those found by Norris,[1] given in Eqs. (36) and (44).

The six solid curves in Fig. 10 show plots of the loss function $L(F)$ numerically calculated from Eqs. (62)–(65) for a range of values of α. As expected, for small values of α the curves lie close to the Norris result for an elliptical cross-section, and for large values of α the curves approach the Norris result for a rectangular cross-section.

E. $J_c(B)$ in the thin-film limit

All the results in this paper have been carried out using the assumption that the critical current density J_c is independent of the local flux density B. To carry out loss calculations when J_c depends strongly upon B requires intensive numerical work, even in the thin-film limit, because the profiles of $B_y(x,0,t)$ and $\bar{J}_z(x,t)$ then must be calculated self-consistently at all times t during the ac cycle. To account approximately for the effect of self-field suppression of $J_c(B)$ upon the ac losses, we can make use of Eqs. (36), (44), and (62)–(65), which assume a constant J_c, by replacing J_c by

$J_{cI}=J_c(B_I)$, where B_I is the average of $B_y(x,0)$ over the flux-penetrated band $c<x<a$ when the peak current is I. From Eqs. (15)–(20) we thus obtain

$$B_I = \frac{1}{a-c}\int_c^a B_y(x,0) \tag{66}$$

$$B_I = \mu_0 J_{cI} b P_\alpha(\tilde{c}), \tag{67}$$

where the function $P_\alpha(\tilde{c})$ and its limits when $\alpha \to 0$ and ∞ are given by

$$P_\alpha(\tilde{c}) = \frac{1}{(1-\tilde{c})\tan^{-1}\alpha}\left[\tanh^{-1}\sqrt{\frac{\alpha^2(1-\tilde{c}^2)}{1+\alpha^2(1-\tilde{c}^2)}} + \frac{\sqrt{1+\alpha^2(1-\tilde{c}^2)}}{\alpha}\tanh^{-1}\sqrt{1-\tilde{c}^2} - \frac{\sqrt{1+\alpha^2}}{\alpha}\tanh^{-1}\sqrt{\frac{(1+\alpha^2)(1-\tilde{c}^2)}{1+\alpha^2(1-\tilde{c}^2)}}\right], \tag{68}$$

$$P_0(\tilde{c}) = \frac{\sqrt{1-\tilde{c}^2} - \tilde{c}^2 \tanh^{-1}\sqrt{1-\tilde{c}^2}}{2(1-\tilde{c})}, \tag{69}$$

$$P_\infty(\tilde{c}) = \frac{2(\sqrt{1-\tilde{c}^2}\tanh^{-1}\sqrt{1-\tilde{c}^2} + \ln\tilde{c})}{\pi(1-\tilde{c})}, \tag{70}$$

and $F=I/I_c$ in Eqs. (16), (18), and (20) must be replaced by $F_I=I/I_{cI}$, where $I_{cI}=S_c J_{cI}$. The transport ac loss per cycle per unit length at each current-peak value I is then approximated by $Q'=\mu_0 I^2 L(F_I)$, where L is given by Eq. (62) for $0<\alpha<\infty$, Eq. (36) for $\alpha=0$, and Eq. (44) for $\alpha=\infty$. We can define L_{eff} making reference to the critical current density $J_{cp}=J_c(B_p)$, where the subscript p refers to full penetration of the strip (i.e., when $\tilde{c}=c/a=0$), where $B_p=\mu_0 J_{cp}bP_\alpha(0)$ and the full-penetration critical current is $I_{cp}=S_c J_{cp}$. As a function of $F_p=I/I_{cp}$, we therefore have

$$L_{eff}(F_p) = \frac{Q'}{\mu_0 I_{cp}^2} = \left(\frac{J_{cI}}{J_{cp}}\right)^2 L\left(F_p \frac{J_{cp}}{J_{cI}}\right). \tag{71}$$

To proceed further, we need an explicit model for the dependence of $J_c(B)$. Choosing the Kim model,

$$J_c(B) = J_c(0)/(1+B/B_0), \tag{72}$$

we can solve Eq. (67) to obtain

$$\frac{J_{cI}}{J_{cp}} = \frac{1+\sqrt{1+4\gamma P_\alpha(0)}}{1+\sqrt{1+4\gamma P_\alpha(\tilde{c})}}, \tag{73}$$

where $\tilde{c}$ is determined as a function of F_p by numerically solving Eq. (16) and (18), or (20) with F replaced by $F_p J_{cp}/J_{cI}$. The dimensionless parameter $\gamma=\mu_0 J_c(0)b/B_0$ is a measure of how strongly J_c depends upon B.

Numerical calculations for various values of α and γ reveal that including the B dependence of $J_c(B)$ does not have a dramatic influence upon $L_{eff}(F_p)$. Shown in Fig. 11 is a plot of the ratio $L_{eff}(F_p)/L(F_p)$ for $\gamma=10$ and values of $\alpha=0$ (elliptical cross-section), 10, 90.3, and ∞ (rectangular cross-section) in the thin-film limit, where $L_{eff}(F_p)$ is given by Eq.

(71) and $L(F_p)$ by Eq. (62). On a log-log plot the power-law dependence of $L_{eff}(F_p)$ differs only slightly from that of $L(F_p)$.

IV. DISCUSSION

In this paper I have addressed the question of whether the ac transport losses in type-II superconducting strips should vary as F^3, F^4, or something in between, where $F=I/I_c$, I is the peak alternating current, and I_c is the critical current. To account for effects of the cross-sectional shape and the thickness dependence of the strips, I did calculations assuming cross-sections whose shapes are modeled by Eq. (1), which, by varying the shape parameter α, describes an ellipse when $\alpha \to 0$, a rectangle when $\alpha \to \infty$, and something in between for intermediate values of α.

In Sec. II A I showed how the vector potential and magnetic field in thick films can be calculated to high accuracy using this function, and in Sec. II B I used the complex-magnetic-field method to calculate the magnetic field and sheet-current density for thin films with cross-sections that are elliptical, rectangular, or something in between. In Sec. III I discussed how to use the magnetic fields obtained as above to calculate hysteretic ac transport losses, beginning with a description of some general loss expressions in Sec. III A.

I addressed the behavior in strips of elliptical cross-section in Sec. III B. In Sec. III B 1 I reviewed the results of Norris[1] and calculated the fraction of losses attributable to the B_y contribution, and in Sec. III B 2 I discussed the origin of the F^3 dependence of the ac losses for small F.

For samples of rectangular cross-section, discussed in Sec. III C, I concluded that the losses should always vary as F^3 for sufficiently small F. However, I found for thin films that there is a relatively large range of values of F for which the losses vary as F^4 and that as the film becomes very thin, the range of values of F for which the F^3 behavior holds becomes very small. In Sec. III C 2 I used a conformal-mapping method to obtain approximations for the F depen-

dence of the ac losses in a rectangular strip, and in Sec. III C 3 I presented plots of numerically calculated ac losses for rectangular strips of various thicknesses, showing the transition between F^3 and F^4 behaviors.

In Sec. III D I calculated the ac losses in very thin strips of intermediate cross-section characterized by the shape parameter α. For the limiting cases of $\alpha=0$ (elliptical cross-section) and $\alpha=\infty$ (rectangular cross-section) my results reduced to those of Norris,[1] but for intermediate values of α the calculated losses were between these two limits.

To investigate to what extent the magnetic-field dependence of the critical current density J_c plays a role, in Sec. III E I used the Kim model to examine the influence of $J_c(B)$ in thin films. I found that while the B dependence does affect the magnitude of the ac losses, it does not have a significant effect upon the F dependence of the losses.

ACKNOWLEDGMENTS

APPENDIX A: ELLIPTICAL CROSS-SECTION

The vector potential generated by a uniform current density J_c flowing in the z direction through a cylinder of elliptical cross-section centered on the z axis, having semimajor axis a along the x axis and semiminor axis b along the y axis is $\boldsymbol{A}_{ce}(x,y)=A_{cze}(x,y)\hat{z}$ [Eq. (5)], where

$$A_{cze}(x,y) = -\frac{\mu_0 J_c(bx^2+ay^2)}{2(a+b)} \tag{A1}$$

on or inside the ellipse $(x/a)^2+(y/b)^2=1$, and

$$A_{cze}(x,y) = -\Re\frac{\mu_0 J_c ab}{2(a^2-b^2)}\left[\zeta(\zeta-\sqrt{\zeta^2-a^2+b^2})\right.$$
$$\left.+(a^2-b^2)\ln\left(\frac{\zeta+\sqrt{\zeta^2-a^2+b^2}}{a+b}\right)\right], \ b\neq a, \tag{A2}$$

$$=-\Re\frac{\mu_0 J_c a^2}{2}\left[\frac{1}{2}+\ln\left(\frac{\zeta}{a}\right)\right], \ b=a, \tag{A3}$$

on or outside the ellipse, where $\zeta=x+iy$ and $\Re$ denotes the real part.

Analytic expressions for the x and y components of the corresponding flux density $\boldsymbol{B}_{ce}(x,y)=\nabla\times\boldsymbol{A}_{ce}(x,y)$ are given in Ref. 1.

APPENDIX B: RECTANGULAR CROSS-SECTION

The vector potential generated by a uniform current density J_c flowing in the z direction through a cylinder of rectangular cross-section centered on the z axis, having width $2a$ along the x axis and height $2b$ along the y axis is $\boldsymbol{A}_{cr}(x,y)=A_{czr}(x,y)\hat{z}$ [Eq. (5)], where

$$A_{czr}(x,y) = \frac{\mu_0 J_c}{4\pi}\left\{(x-a)^2\left[\tan^{-1}\left(\frac{y+b}{x-a}\right)-\tan^{-1}\left(\frac{y-b}{x-a}\right)\right]\right.$$
$$+(x+a)^2\left[\tan^{-1}\left(\frac{y-b}{x+a}\right)-\tan^{-1}\left(\frac{y+b}{x+a}\right)\right]$$
$$+(y-b)^2\left[\tan^{-1}\left(\frac{x+a}{y-b}\right)-\tan^{-1}\left(\frac{x-a}{y-b}\right)\right]$$
$$+(y+b)^2\left[\tan^{-1}\left(\frac{x-a}{y+b}\right)-\tan^{-1}\left(\frac{x+a}{y+b}\right)\right]$$
$$+(x-a)(y+b)\ln[(x-a)^2+(y+b)^2]$$
$$-(x-a)(y-b)\ln[(x-a)^2+(y-b)^2]$$
$$+(x+a)(y-b)\ln[(x+a)^2+(y-b)^2]$$
$$-(x+a)(y+b)\ln[(x+a)^2+(y+b)^2]$$
$$+4a^2\tan^{-1}\left(\frac{b}{a}\right)+4b^2\tan^{-1}\left(\frac{a}{b}\right)$$
$$\left.+4ab\ln(a^2+b^2).\right\} \tag{B1}$$

The x and y components of the corresponding flux density $\boldsymbol{B}_{cr}(x,y)=\nabla\times\boldsymbol{A}_{cr}(x,y)$ are

$$B_{cxr}(x,y) = \frac{\mu_0 J_c}{4\pi}\left\{2(y-b)\left[\arctan\left(\frac{x+a}{y-b}\right)-\arctan\left(\frac{x-a}{y-b}\right)\right]\right.$$
$$+2(y+b)\left[\arctan\left(\frac{x-a}{y+b}\right)-\arctan\left(\frac{x+a}{y+b}\right)\right]$$
$$+(x+a)\ln\left[\frac{(x+a)^2+(y-b)^2}{(x+a)^2+(y+b)^2}\right]$$
$$\left.+(x-a)\ln\left[\frac{(x-a)^2+(y+b)^2}{(x-a)^2+(y-b)^2}\right]\right\}, \tag{B2}$$

$$B_{cyr}(x,y) = \frac{\mu_0 J_c}{4\pi}\left\{2(x-a)\left[\arctan\left(\frac{y-b}{x-a}\right)-\arctan\left(\frac{y+b}{x-a}\right)\right]\right.$$
$$+2(x+a)\left[\arctan\left(\frac{y+b}{x+a}\right)-\arctan\left(\frac{y-b}{x+a}\right)\right]$$
$$+(y-b)\ln\left[\frac{(x-a)^2+(y-b)^2}{(x+a)^2+(y-b)^2}\right]$$
$$\left.+(y+b)\ln\left[\frac{(x+a)^2+(y+b)^2}{(x-a)^2+(y+b)^2}\right]\right\}. \tag{B3}$$

APPENDIX C: NUMERICAL CALCULATION OF $B_I(x,y)$

The auxiliary magnetic induction $\boldsymbol{B}_I(x,y)=\nabla\times\boldsymbol{A}_I(x,y)$ [see Eq. (9)] is generated by a uniform current density $J_z=-J_c$ flowing only in the cross-section S_I. The x and y components of $\boldsymbol{B}_I(x,y)$ readily can be calculated numerically from the following one-dimensional integrals:

$$B_{Ix}(x,y) = \frac{\mu_0 J_c}{4\pi} \int_{-c}^{c} \ln\left\{ \frac{(u-x)^2 + [y_I(u) + y]^2}{(u-x)^2 + [y_I(u) - y]^2} \right\} du, \tag{C1}$$

$$B_{Iy}(x,y) = \frac{\mu_0 J_c}{4\pi} \int_{-y_0}^{y_0} \ln\left\{ \frac{[x_I(v) - x]^2 + (v-y)^2}{[x_I(v) + x]^2 + (v-y)^2} \right\} dv, \tag{C2}$$

where the functions $y_I(x)$ and $x_I(y)$ are given in Eqs. (6) and (7).

---

[1] W. T. Norris, J. Phys. D **3**, 489 (1970).

[2] H. R. Kerchner, D. P. Norton, A. Goyal, J. D. Budai, D. K. Christen, D. M. Kroeger, E. D. Specht, Q. He, M. Paranthaman, D. F. Lee, B. C. Sales, F. A. List, and R. Feenstra, Appl. Phys. Lett. **71**, 2029 (1997).

[3] D. Miyagi, O. Tsukamoto, and M. Ciszek, IEEE Trans. Appl. Supercond. **11**, 2449 (2001).

[4] A. M. Campbell and J. E. Evetts, Adv. Phys. **21**, 199 (1972).

[5] E. H. Brandt and M. Indenbom, Phys. Rev. B **48**, 12893 (1993).

[6] E. Zeldov, J. R. Clem, M. McElfresh, and M. Darwin, Phys. Rev. B **49**, 9802 (1994).

[7] J. Rhyner, Physica C **377**, 56 (2002).

[8] R. P. Huebener, R. T. Kampwirth, and J. R. Clem, J. Low Temp. Phys. **6**, 275 (1972).

[9] L. D. Landau, E. M. Lifshitz, and L. P. Pitaevskii, *Electrodynamics of Continuous Media*, 2nd ed. (Elsevier, Amsterdam, 1993).

[10] R. V. Churchill, *Introduction to Complex Variables and Applications* (McGraw-Hill, New York, 1948).

[11] H. Kober, *Dictionary of Conformal Representations* (Dover, Mineola, New York, 1957).

[12] P. F. Byrd and M. D. Friedman, *Handbook of Elliptic Integrals for Engineers and Scientists* (Springer, Berlin, 1971), p. 8.

[13] I. S. Gradshteyn and I. M. Ryzhik, *Table of Integrals, Series, and Products*, 6th ed. (Academic, San Diego, 2000), p. 851.